International Forum on Aeroelasticity and Structural Dynamics
IFASD 2024
17-21 June 2024, The Hague, The Netherlands

ANALYSIS OF INERTIAL GUST LOAD RELIEF CHARACTERISTICS OF HIGH ASPECT RATIO WINGS

Sanuja D. Jayatilake, Mark Lowenberg, Benjamin K. S. Woods, Branislav Titurus

School of Civil, Aerospace and Design Engineering, University of Bristol, Bristol. BS8 1TR. United Kingdom.

Keywords: Gust loads, Inertial load relief, Anti-resonance

Abstract: This paper conceptually explores the potential of exploiting resonant and anti-resonant interactions of force transmissibility functions to suppress responses under external (gust-like) excitation in High Aspect Ratio Wings (HARW). By considering a half-fuselage and wing configuration with a strut incorporating an inerter, it is shown numerically that the anti-resonant regions of the inertial load response of the fuselage can be tailored by augmenting the inertial characteristics of the original configuration. Whilst this was parametrically achieved by varying the inertance of the strut-device, the analytical examination of the underlying contributing factors to anti-resonance recognized a significant influence from the high-frequency non-resonant modes. The demonstrated approach, which achieved frequency-localized suppression of the fuselage responses, could improve ride comfort and reduce specific structural load transmission in HARW aircraft. At the same time, it is stipulated that the same modal inertia-based response tailoring could be aimed at reducing variety of other critical loads such as wing root bending moments.

1 INTRODUCTION

The investigation of gust load reduction methods continues to take a significant place among research and development centered around HARW aircraft. Particularly over the past few decades, a wide range of passive approaches incorporating dynamic absorber devices [1], various articulating devices and reconfiguration approaches [2], and a multitude of other methods [3] have been proposed. Among these, a recently proposed approach aimed at hinged wing configurations showed the potential of exploiting the inertial loads associated with the wing's movement [4] to alleviate the wing root load transmission. This paper explores the inertia-driven augmentation of the wing root load transmission characteristics in the context of the continuous HARW-like structure.

The analysis of the gust responses of elastic aircraft dates to 1932 to the works of Küssner. During discrete gust encounters, an elastic structure exhibits responses comprising of several aeroelastic modes. As a result, selected response components can be highly sensitive to the intricate loading patterns associated with a range of modes, as suggested by the observation surrounding ride comfort study in [6], which examined this behavior under a range of wing flexibility levels. From a frequency domain perspective, when excited at frequencies in the vicinity of a resonant mode, the influence of the non-resonant modes manifests as parasitic or background flexibility effects.

Given an observed response of interest, the non-resonant participation may either be in phase (constructively participating, increasing the net response), or in anti-phase where the non-resonant component reduces the net response. The anti-resonance phenomena seen the in the frequency response functions are typically a result of this multi-modal property, where at specific frequencies the multi-modal superposition essentially results in a complete annihilation of the net response [5].

Assigning anti-resonance at critical operational frequencies is widely exploited in vibration control problems. A classic example of this principle can be associated with the tuned vibration absorber [6-7]. In this case, anti-resonance is introduced by means of an added degree of freedom whose frequency is carefully tuned to place the anti-resonance at the desired operational frequency. As a result, at the anti-resonance, the intricate superposition of the in-phase and out-of-phase modes results in a net zero displacement of the primary degree of freedom. Extending beyond this classical approach, means of assigning the anti-resonance properties without the inclusion of additional degrees of freedom have been widely investigated. Typically, these tend to be centered around active control approaches, where the desired anti-resonance behavior is induced by means of an adopted control scheme. However, it is also recognized that this can be achieved through the careful modifications of the structure itself (e.g., by altering the mass distribution) to achieve the desired eigenfrequencies and vectors [9].

By augmenting the inertial properties of the wing, this paper intends to explore the possibility of modulating the anti-resonant response features of a flexible wing and fuselage configuration subject to harmonic loading. To demonstrate this in a conceptual setting focusing on the structural behavior, the gust excitation is simplified and represented as a distributed shear load applied on the wing without any aerodynamic influences. Additionally, to parametrically drive the anti-resonant characteristics, the inertial augmentation in this work is introduced by means of an inerter device. This essentially entails an effective and directed mass-intensification mechanism realized through kinematic amplification of the input motion and has been the basis of a wide range of modern passive vibration control solutions [10]. This study is focused on the net shear load transmission to the fuselage, which is equivalent to the inertial force from the fuselage acceleration. Hence, this is used as a useful indication of gains in ride quality and other favorable opportunities such as hydrogen fuel storage in the fuselage.

The study in this paper is arranged as follows. The configurational details of the studied problem and the mathematical modelling are described in section 2. The inertially-driven anti-resonant and resonant interactions are initially introduced through a parametric study in section 3.1. The phenomena contributing to the anti-resonant features are then analytically studied in section 3.2, recognizing the potential opportunities arising from the non-resonant modal flexibility. The study concludes after a brief analysis of the internal shear transmission component redistribution under the conditions where the desired suppression is realized.

2 PROBLEM DESCRIPTION

2.1 Bending wing and plunging fuselage configuration

Aiming to reflect the coupled dynamics between the free-body motion of the fuselage and the elastic deflections of the wing, this research explores a half-fuselage and wing configuration illustrated in Figure *1*. The primary objective of this setup is to examine the interactions between

the inertial forces arising from the combined accelerations from the wing's deflections and the plunging motion of the fuselage.

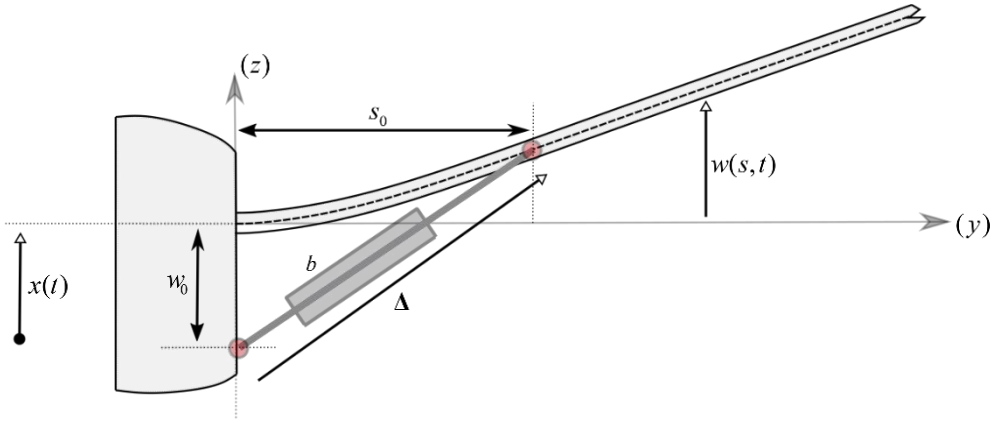

Figure 1 Half span wing-fuselage HARW-like configuration with the strut-based inerter.

To achieve this in a minimal representative configuration and to enable analytical explorations of the underlying phenomena, the problem considered herewith is solely limited to the transversal bending dynamics of the elastic wing. In addition to this, to further elaborate the effects of the inertial forces on the system's responses, a linear inerter is considered, realized in the form of a telescoping strut, as shown in the figure. The physical parameters for the wing are adopted from [11], which entails a representative HARW platform applicable to HALE aircraft.

The described system, along with the coordinate systems are detailed in the figure. The vertical motion of the fuselage of mass $m_{fus} = 25\,\mathrm{kg}$, is described by $x(t)$, and the relative transversal displacement of the wing at a distance s from the wing root is given by $w(s,t)$. These bending displacements are discretized using a family of N shape functions $\mathbf{Y}(s) = \begin{bmatrix} Y_1(s) & \cdots & Y_N(s) \end{bmatrix}^{\mathrm{T}}$. This deformation is then described using a set of time-varying generalized coordinates, $\mathbf{q}(t)$,

$$w(s,t) = \mathbf{Y}(s)^{\mathrm{T}}\mathbf{q}(t). \tag{1}$$

Scaled Chebyshev polynomials are used in this work to construct the basic functions, with the imposed scaling enforcing the kinematic boundary conditions (zero displacement and the gradient) at the wing root. In addition to N-1 Chebyshev polynomials, a synthesised shape function is included (within the same N sized basis), which is derived from the static solution to the problem with the beam being subjected to a point shear load at the location of the attachment of the inerter-strut. This is done to essentially include sufficient information in the higher order spatial derivatives in the basis function set, such that the discrete loading effects at the inerter attachment point are effectively captured. This artificially generated shape function takes the form:

$$Y_N(s) = \begin{cases} s^2 - \dfrac{1}{3s_0}s^3, & s < s_0 \\ \dfrac{2s_0^2}{3} + s_0\left(s - s_0\right), & s_0 < s < L \end{cases} \tag{2}$$

This additional function essentially incorporates a discontinuity in the term contributing to the internal shear load distribution, whilst enforcing geometrical continuity (gradient and displacement) at the strut-attachment location.

2.2 Generalized mathematical model

The equations of motions describing the generalized coordinates of the half-fuselage and wing are developed using the energy-based approach utilizing the Lagrangian equation of the second kind. The potential and kinetic energies of the wing can be expressed as follows:

$$U_K = \frac{1}{2}\int_0^L EIw''(s,t)^2\,ds, \qquad U_T = \frac{1}{2}\int_0^L m\left(\dot{w}(s,t)+\dot{x}(t)\right)^2 ds + \frac{1}{2}m_{fus}\dot{x}(t)^2 \tag{3}$$

where $EI = 2\times10^4\ \mathrm{Nm}^2$ is the bending rigidity, $m = 0.75\,\mathrm{kg/m}$ is the mass per unit length, and $L = 16\,\mathrm{m}$ is the semi-span of the wing. On applying the Lagrangian operator, the equations of motion can be derived as follows,

$$\begin{bmatrix}\mathbf{M} & \mathbf{g}\\ \mathbf{g}^{\mathrm{T}} & m_{fus}\end{bmatrix}\begin{bmatrix}\ddot{\mathbf{q}}\\ \ddot{x}\end{bmatrix}+\begin{bmatrix}\mathbf{D} & \\ & 0\end{bmatrix}\begin{bmatrix}\dot{\mathbf{q}}\\ \dot{x}\end{bmatrix}+\begin{bmatrix}\mathbf{K} & \\ & 0\end{bmatrix}\begin{bmatrix}\mathbf{q}\\ x\end{bmatrix}=\begin{bmatrix}\mathbf{Q}_b^{(q)}+\mathbf{Q}_{ext}^{(q)}\\ \mathbf{Q}_b^{(x)}+\mathbf{Q}_{ext}^{(x)}\end{bmatrix} \tag{4}$$

In the above, the effects of the inerter and external loading applied are described using the generalized forces $\mathbf{Q}$. The matrices $\mathbf{M}$ and $\mathbf{K}$, respectively, are the mass and the stiffness matrices of the wing for the case when the fuselage is constrained, given by,

$$\mathbf{M} = \left(\int_0^L \rho\,\mathbf{Y}\mathbf{Y}^{\mathrm{T}} ds\right), \qquad \mathbf{K} = \left(\int_0^L EI\,\mathbf{Y}''\mathbf{Y}''^{\mathrm{T}} ds\right) \tag{5}$$

and $\mathbf{g}$ is the inertial term coupling the vertical motion of the fuselage with the acceleration due to the wing's deflections, given by,

$$\mathbf{g} = \left(\int_0^L m\,\mathbf{Y}\,ds\right) \tag{6}$$

and finally, $\mathbf{D}$ is the wing damping matrix described here as a linear combination of the wing mass and the stiffness matrices, $\mathbf{D} = \alpha\mathbf{M} + \beta\mathbf{K}$. In this work, the pair of values $\alpha = 0.1, \beta = 0.001$ was chosen to yield the damping ratios in the range 1%-2% on the first two bending modes. The modelling of the inerter, the external forcing applied in the presented study and the force transmissibility definitions are described in the next sections.

2.3 Generalized forces due to inerter and external loading

Figure *2* shows the details of the internal forces transmitted through the strut and the wing root. As shown, the inerter-driven force, F_b, acts through the line of the strut. More specifically, the line of action of this force coincides with $\mathbf{\Lambda}$ vector (see Figure *1*), and this vector can be described in the moving frame of reference as follows,

$$\boldsymbol{\Delta} = \begin{bmatrix} s_0 \\ w(s_0,t) + w_0 \end{bmatrix} \tag{7}$$

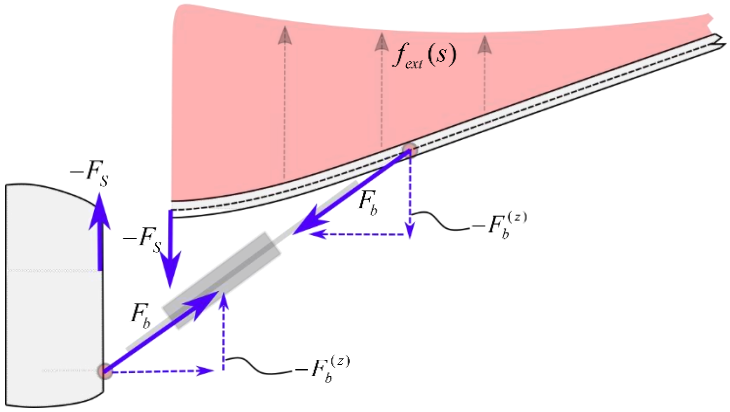

Figure 2 Forces in the shear (transversal) direction.

To develop the link between the extension of the strut and the inerter force, first the variation of $\boldsymbol{\Delta}$ and its Euclidean length, $|\boldsymbol{\Delta}|$, is considered under an infinitesimal displacement of the wing, $\delta\mathbf{q}$. It can be shown that,

$$\begin{aligned} \delta\boldsymbol{\Delta} &= \begin{bmatrix} 0 \\ \delta w_{s=s_0} \end{bmatrix} = \begin{bmatrix} 0 \\ \mathbf{Y}^{\mathrm{T}}(s_0)\,\delta\mathbf{q} \end{bmatrix} \\ \delta|\boldsymbol{\Delta}| &= \frac{w_0}{|\boldsymbol{\Delta}_0|}\delta w_{s=s_0} = \frac{w_0}{|\boldsymbol{\Delta}_0|}\mathbf{Y}^{\mathrm{T}}(s_0)\,\delta\mathbf{q} \end{aligned} \tag{8}$$

where $|\boldsymbol{\Delta}_0|$ is the equilibrium length. Using the above expressions, and under the assumption of linearity (correct to up to the first order variations), the force through the inerter can be written as follows,

$$F_b = b\frac{\mathrm{d}^2|\boldsymbol{\Delta}|}{\mathrm{d}t^2} = -b\,\mathbf{V}^{\mathrm{T}}\ddot{\mathbf{q}} \tag{9}$$

where,

$$\mathbf{V} = -\frac{w_0\mathbf{Y}(s_0)}{|\boldsymbol{\Delta}_{\mathbf{q}=\mathbf{0}}|} \tag{10}$$

Note that the signage selected for the above definition is arbitrarily chosen, in this case such that all additional contributions to the mass matrix have positive signs.

Noting that the normalized line of action of the inerter force can be described by, $\boldsymbol{\Delta}/|\boldsymbol{\Delta}|$, after projecting this force on infinitesimal displacements at the point of action on the wing and on the fuselage, the infinitesimal work imparted on the them can be derived:

$$\delta \mathbf{q}^{\mathrm{T}} \mathbf{Q}_b^{(q)} = -\left(F_b \frac{\mathbf{\Delta}}{|\mathbf{\Delta}|} \right)^{\mathrm{T}} \delta \mathbf{\Delta}, \qquad \delta x \mathbf{Q}_b^{(x)} = +\left(F_b \frac{\mathbf{\Delta}}{|\mathbf{\Delta}|} \right)^{\mathrm{T}} \begin{bmatrix} 0 \\ \delta x \end{bmatrix} \tag{11}$$

Accordingly, continuing to retain up to and including the first order (i.e., linear) terms, the above generalised forces can be identified as follows,

$$\mathbf{Q}_b^{(q)} = -b\left(\mathbf{V}\mathbf{V}^{\mathrm{T}}\right)\ddot{\mathbf{q}}, \qquad \mathbf{Q}_b^{(x)} = -b\left(\frac{w_0}{|\mathbf{\Delta}_{\mathbf{q}=\mathbf{0}}|} \right)\mathbf{V}^{\mathrm{T}}\ddot{\mathbf{q}} \tag{12}$$

Note that in the above, $\mathbf{Q}_b^{(x)}$ is essentially the component of the inerter force in the vertical (z) direction, (indicated as $-F_b^{(z)}$ in Figure *2*), such that $-F_b^{(z)} = (w_0 / |\mathbf{\Delta}_{\mathbf{q}=\mathbf{0}}|)F_b$. To develop the internal force transmissibility characteristics in the frequency domain, this work assumes an external loading in the form of a distributed elliptical shear load applied on the wing. This is introduced through the following load distribution, also indicated in Figure *2*,

$$f_{ext}(s) = F_{ext} \frac{\sqrt{1-(s/L)^2}}{\int_0^L \sqrt{1-(\tilde{s}/L)^2}\, d\tilde{s}} \tag{13}$$

Note that the force distribution is normalized such that the total vertical shear load is equal to F_{ext}. The corresponding generalized forces can be compiled as follows,

$$\mathbf{Q}_{ext}^{q} = \int_0^L f_{ext}\mathbf{Y}\, ds = F_{ext} \frac{\int_0^L \mathbf{Y}(s)\sqrt{1-(s/L)^2}\, ds}{\int_0^L \sqrt{1-(s/L)^2}\, ds}, \quad \mathbf{Q}_{ext}^{x} = F_{ext} \tag{14}$$

2.4 Output force transmissibility definition under harmonic excitation

To obtain the frequency domain responses, harmonic forcing is assumed in the form, $F_{ext} = \hat{F}_{ext} e^{\mathrm{i}\omega t}$, with the responses $\mathbf{q} = \hat{\mathbf{q}}(\omega)e^{\mathrm{i}\omega t}$, $x = \hat{x}(\omega)e^{\mathrm{i}\omega t}$ at the driving frequency ω. Under this input, the output of the structural coordinates, $\hat{\mathbf{q}}(\omega)$, and the fuselage displacement, $\hat{x}(\omega)$, are initially obtained from the frequency-domain representation of Eq.(4). Given the particular interest surrounding the internal forces transmitted under the specific loading, the corresponding representation of these forces in the form of the transmissibility functions are derived from the above displacements. The inertial and elastic forces in the transversal direction considered herein are summarized in Table *1*.

The corresponding force transmissibility functions involve the above force components expressed in a ratio relative to the input force (e.g., the wing root shear force transmissibility is defined as $H_{F_S}(\omega) = \hat{F}_S(\omega) / \hat{F}_{ext}$).

Table 1 Internal transversal (shear) force components used to analyze the structural response.

Description	Mathematical expression (frequency domain)
Wing root shear force	$\hat{F}_S(\omega) = EI\ \mathbf{Y}'''(0)^{\mathrm{T}}\hat{\mathbf{q}}(\omega)$
Strut (inerter) force (shear component)	$\hat{F}_b^{(z)}(\omega) = -\omega^2 b\,(w_0 / \lvert\boldsymbol{\Delta}_{\mathbf{q}=\mathbf{0}}\rvert)\mathbf{V}^{\mathrm{T}}\hat{\mathbf{q}}(\omega)$
Inertial force – wing acceleration	$\hat{I}_w(\omega) = -\omega^2\,\mathbf{g}^{\mathrm{T}}\hat{\mathbf{q}}(\omega) - \omega^2 mL\,\hat{x}(\omega)$
Inertial force – fuselage acceleration	$\hat{I}_{fus}(\omega) = -\omega^2 m_{fus}\hat{x}(\omega)$

3 RESULTS

3.1 Numerical observations

Figure *3* shows the fuselage inertial force transmissibility function, $H_{I_{fus}}$, under the external shear loading exerted on the wing. Note that, this inertial force response is directly proportional to the acceleration response of the fuselage. Hence, the resonant and the anti-resonant behavior of the inertial force transmissibility function reflects that of the accelerance function (the ratio between the acceleration response and the input force in frequency domain).

As illustrated by Figure *3*(a), the resonant regions in the considered response function appear at the natural frequencies of the coupled wing-fuselage system. The first three oscillatory modes are shown in the studied frequency range (B1-B3), which comprise of coupled wing bending and fuselage plunging activity. Under increasing levels of inertance, *b*, these frequencies exhibit a general reduction due to the progressive inertial amplification effect.

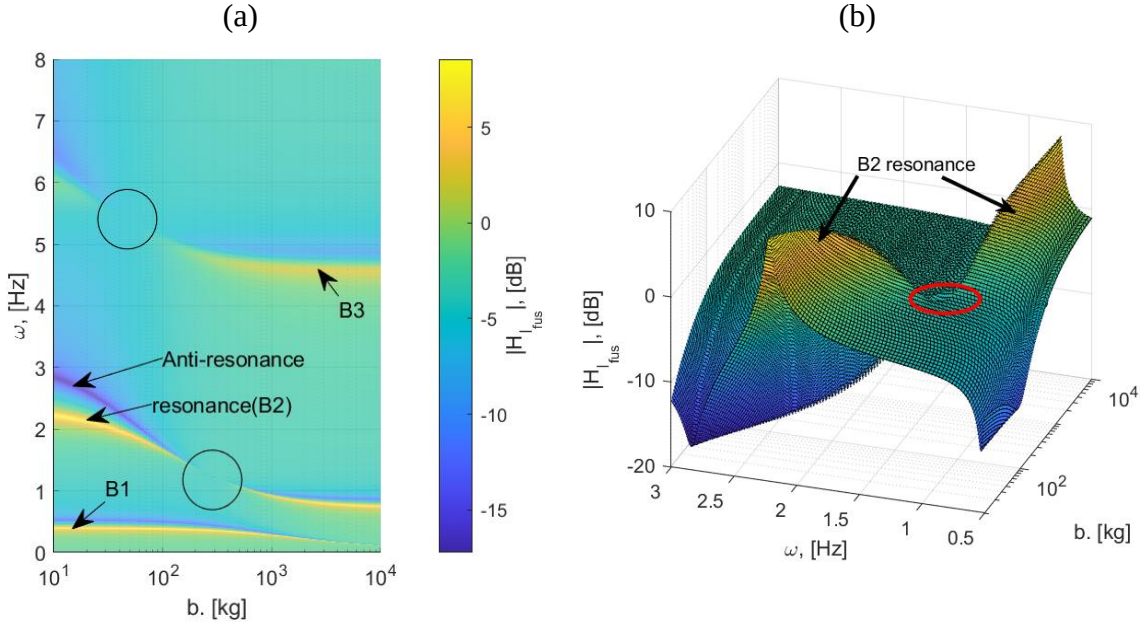

Figure 3 Transmissibility function of the fuselage inertial force response under shear forcing applied on the wing. (a) Scalar plot of magnitudes. (b) Zoomed in view around the second bending mode's (B2) frequency.

At the same time, the anti-resonance phenomena appear in the form of dark (blue) regions in the figure and correspond to the inertance-frequency combinations at which the fuselage exhibits minimal I_{fus} responses, indicating minimal accelerations. As the inertance is progressively increased, the anti-resonance frequencies exhibit a reduction which results in an intercept with the resonant regions at the specific levels of inertances. These regions, corresponding to the B2 and B3 modes, are encircled in Figure *3* (a). Within these regions, the resonant and anti-resonant interactions coalesce and, essentially, annihilate each other. This is further illustrated for the case of the B2 mode in Figure *3* (b). This phenomenon, which results in no net resonant amplification of the fuselage inertial force response in the specified frequency regions, can be exploited to enhance the ride comfort under broadband gust excitation and/or to avoid excessive force-transmission across selected structural components.

3.2 Analytical exploration of anti-resonance drivers

The contributing physical phenomena, not limited to the inerter-driven dynamics, which drive the anti-resonance and resonance interactions are further explored analytically in this section. This analysis is developed by examining the participation of the system of the generalized modal coordinates corresponding to the modal basis of the wing-domain. The modal basis in question is specified under fixed-fuselage conditions, and then, their coupled participation under the free-fuselage conditions. The intended outcome is the analytical identification of the inerter-driven effects contributing to the anti-resonance phenomena, and more importantly, the effects of the background flexibility arising from the non-resonant modes.

To begin this development, first the mass-normalized modal basis $\begin{bmatrix}\boldsymbol{\varphi}_1 & \cdots & \boldsymbol{\varphi}_N\end{bmatrix}$ of the wing beam with the inerter and with the fuselage constrained is obtained by solving the eigenvalue problem corresponding to this sub-system,

$$\left(\mathbf{M}+b\mathbf{V}\mathbf{V}^{\mathrm{T}}\right)\ddot{\mathbf{q}}+\mathbf{D}\dot{\mathbf{q}}+\mathbf{K}\mathbf{q}=\mathbf{Q}_{ext}^{(q)} \tag{15}$$

Considering the mass normalized quality of the obtained basis, along with the identified modal frequencies and damping ratios, ω_j, ς_j, the problem can be re-written in a decoupled format using the modal coordinates $\boldsymbol{\lambda}$ such that $\mathbf{q}=\begin{bmatrix}\boldsymbol{\varphi}_1 & \cdots & \boldsymbol{\varphi}_N\end{bmatrix}\boldsymbol{\lambda}$ and

$$\ddot{\lambda}_j+2\varsigma_j\omega_j\dot{\lambda}_j+\omega_j^2\lambda_j=p_j \tag{16}$$

In the above formulation, p_j are the corresponding modal loads from the external excitation, such that $p_j=\boldsymbol{\varphi}_j^{\mathrm{T}}\mathbf{Q}_{ext}^{(q)}$.

Due to the intrinsic relationships and the boundary conditions which govern the cantilevered beam with the fixed fuselage associated with Eq.(16), the modal shear load S_j transmitted at the wing root can be written in the form,

$$S_j=k_j\lambda_j=-\left(I_j+k_{b_j}\right)\ddot{\lambda}_j \tag{17}$$

where $I_j\ddot{\lambda}_j$ and $k_{b_j}\ddot{\lambda}_j$, respectively, are the modal inertial loads arising from the inertia of the wing itself and that of the inerter. The above is written assuming minimal shear-wise loading

originating from the synthesized damping matrix, based on the premise of small structural damping ratios.

These terms take the form,

$$I_j = \boldsymbol{\varphi}_j^{\mathrm{T}}\mathbf{g}, \qquad k_{b_j} = -b\left(\frac{w_o}{\left|\boldsymbol{\Delta}_{\mathbf{q}=\mathbf{0}}\right|}\right)\left(\mathbf{V}^{\mathrm{T}}\boldsymbol{\varphi}_j\right) \tag{18}$$

Note that the terms $\mathbf{g}, \mathbf{V}$ are defined previously in section 2.2. Accordingly, considering harmonic motion at the resonant frequency of the respective mode yields the following,

$$k_j = \omega_j^2\left(I_j + k_{b_j}\right) \tag{19}$$

The above inertial and shear force terms can be used to describe the coupled equations of motion with the plunging fuselage. This is done by adding the inertial force due to the acceleration at the root in Eq.(16) and by balancing the totality of the wing root modal shear forces with the inertial force due to the fuselage acceleration.

$$\begin{aligned} &\ddot{\lambda}_j + 2\varsigma_j\omega_j\dot{\lambda}_j + \omega_j^2\lambda_j = -I_j\ddot{x} + p_j \\ &m_{fus}\ddot{x} = \sum_{j=1}^{N} k_j\lambda_j + \sum_{j=1}^{N} k_{b_j}\ddot{\lambda}_j \end{aligned} \tag{20}$$

It is worth mentioning that the above system of equations ultimately describes the same problem dictated by Eq.(4). A key difference between the two equations is the means by which the fuselage degree of freedom and the wing's deflection are coupled. In the model (Eq.(4)), the last equation considers the force balance on the entire wing-fuselage assembly, with the acceleration of the two systems generating coupling in the mass matrix. In the above (Eq.(20)), the inertial force due to the fuselage acceleration is equated to the total shear load transmitted through the wing root and the inerter.

By substituting the definition from Eq.(19) and the response in terms of the modal coordinates based on the first equation in Eq.(20), the fuselage inertial force response in the frequency domain can be written as,

$$\hat{I}_{fus} = -\omega^2 m_{fus}\hat{x} = \frac{\displaystyle\sum_{j=1}^{N} p_j\left(\frac{\omega_j^2\left(I_j + k_{b_j}\right) - \omega^2 k_{b_j}}{P_j(\omega)}\right)}{1 + \displaystyle\sum_{j=1}^{N}\mu_j\left(\frac{\omega_j^2\left(I_j + k_{b_j}\right) - \omega^2 k_{b_j}}{P_j(\omega)}\right)} \tag{21}$$

where $\mu_j = I_j / m_{fus}$ is the modal shear inertia ratio normalised by the fuselage mass, and $P_j(\omega) = \omega_j^2 + 2\mathrm{i}\varsigma_j\omega_j\omega - \omega^2$ are the characteristic polynomials of the fixed-fuselage wing, each admitting the poles corresponding to the mode as a root. To analytically approach the interactions between the anti-resonance and resonance regions of the above transfer function, Eq.(21) is further

simplified considering a frequency-localised region around a selected mode. Accordingly, the frequency region $\omega \approx \omega_R$, about a selected mode $j=R$ is selected to develop the analysis.

Firstly, it is assumed that the natural frequencies only vary minimally between the fixed-fuselage and free-fuselage cases. That is, once the coupled fuselage-wing dynamics is considered, the resonant region is assumed to lie in the vicinity of the frequency ω_R itself. Secondly, sufficient separation in the natural frequencies is assumed between the cantilever modes, $\omega_{j+1} \gg \omega_j$. Finally, for the purpose of this analysis, small damping ratios are assumed.

The resonant and anti-resonant regions of the transfer function in Eq.(21) are manifested as a result of the excitation frequency approaching its poles and zeros, respectively. To identify the characteristic polynomial of the mode R under free-fuselage conditions, which admits the respective pole as a solution in the denominator of Eq.(21), its numerator and the denominator is multiplied by $P_R(\omega)$. At the same time, under the assumption of small damping ratios, $P_j(\omega) \approx \omega_j^2 - \omega^2,\ j \neq R$ is assumed.

$$\hat{I}_{fus} \approx \frac{p_R\left(\omega_R^2\left(I_R + k_{b_R}\right) - \omega^2 k_{b_R}\right) + P_R(\omega)\sum_{j\neq R} p_j\left(\dfrac{\omega_j^2\left(I_j + k_{b_j}\right) - \omega^2 k_{b_j}}{\omega_j^2 - \omega^2}\right)}{\mu_R\left(\omega_R^2\left(I_R + k_{b_R}\right) - \omega^2 k_{b_R}\right) + P_R(\omega)\left[1 + \sum_{j\neq R}\mu_j\left(\dfrac{\omega_j^2\left(I_j + k_{b_j}\right) - \omega^2 k_{b_j}}{\omega_j^2 - \omega^2}\right)\right]} \tag{22}$$

Next, under the frequency separation assumption, the following can be suggested,

$$\frac{-\omega^2}{\omega_j^2 - \omega^2} \approx \begin{cases} 1, & j < R \\ 0, & j > R \end{cases}, \quad \frac{\omega_j^2}{\omega_j^2 - \omega^2} \approx \begin{cases} 0, & j < R \\ 1, & j > R \end{cases} \tag{23}$$

With the above approximations, the frequency corresponding to the anti-resonance can be obtained by seeking the zero from the solution of the numerator in Eq.(22). Note that, assuming low damping, only the real component of this condition is satisfied.

$$\omega_{anti-res}^2 \approx \omega_R^2\left(1 + \frac{I_R}{k_{b_R} + \sum_{j=R+1}^{N}\frac{p_j}{p_R}I_j + \sum_{j=1}^{R-1}\frac{p_j}{p_R}k_{b_j}}\right) \tag{24}$$

Prior to inferring useful information from this approximate equation, it must be noted that no assumption was made about the existence of an anti-resonant frequency in the vicinity of the considered frequency range about a mode R. The solution given above is simply the zero admitted by the transfer function derived in this manner. Additionally, as opposed to the resonant frequencies, the anti-resonance frequency is depended on the form of excitation used, which the above equation implies through the presence of the p_j / p_R term. For the case with no inerter (all $k_{b_j} = 0$), the general structure of the above solution suggests the likelihood of the presence of an

anti-resonance solution in the vicinity of a low frequency mode, provided that modal shear inertia (I_R) of the resonant mode in question is comparably small to the aggregation of the same quantity of the higher-frequency modes, scaled by the excitation dependent weighing p_j / p_R. This feature facilitates previously observed beneficial inerter-driven resonance and anti-resonance interactions, as the anti-resonance frequency is nominally placed closed to the resonant region.

The contributing terms which determine the frequency of anti-resonance can be identified. Notably, aside from the effect of the inerter on the resonant mode R (k_{b_R}) , the higher-frequency cantilever modes contribute through the shear-wise inertial forces. Their participation is subjected to the weighing (p_j / p_R) associated with the ratio of the forcing on the non-resonant modes and the forcing on the mode in the resonant region itself. Hence, for instance, if a certain higher frequency non resonant mode is not sufficiently activated by the imposed forcing, then the shear inertia associated with that mode cannot tailor the anti-resonant behaviour in question.

To examine the underlying changes observed on the shear force transmission through the wing root and through the inerter, Figure *4* shows the respective force transmissibility functions (H_{F_S} and $H_{F_b^{(z)}}$) under varying levels of inertance. To provide a comparison against the levels of inertance at which the beneficial resonant and anti-resonant interactions were observed on $H_{I_{fus}}$, the anti-resonance frequencies of this function are overlaid on the illustrated force transmissibility function. The anti-resonant frequencies are generated numerically from the results in Figure *3* (by picking the troughs), are compared against that obtained analytically from Eq.(24), to ascertain the validity of the analytical approximation.

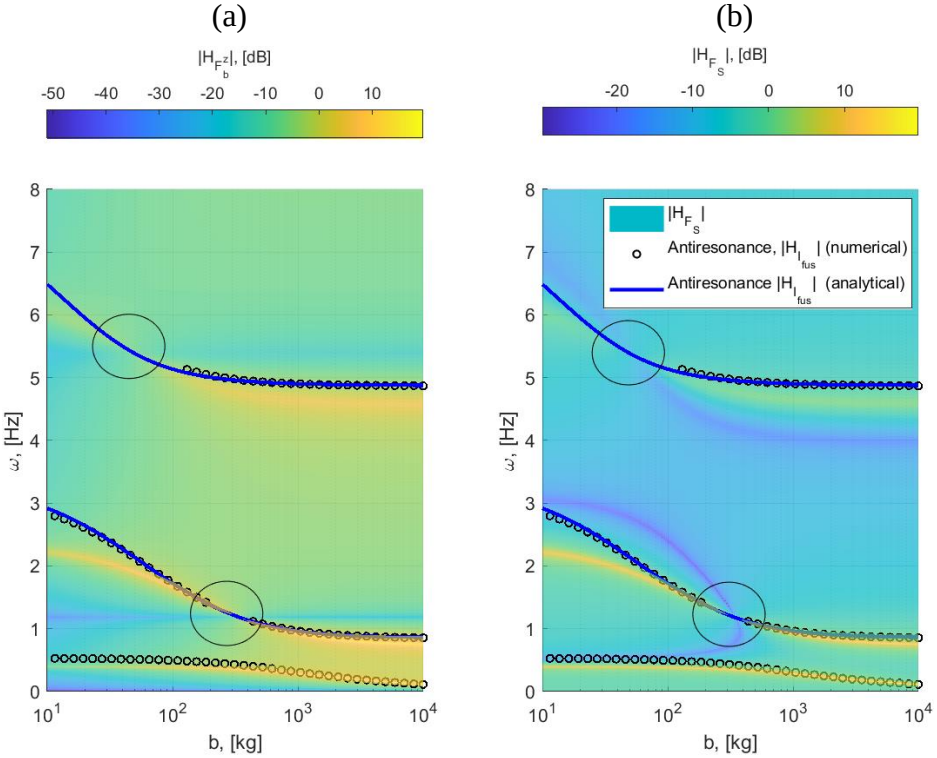

Figure 4 Transfer functions of the fuselage load components with the antiresonance regions of the fuselage acceleration response overlaid (bird's view projection). (a) Inerter force. (b) Wing root shear force.

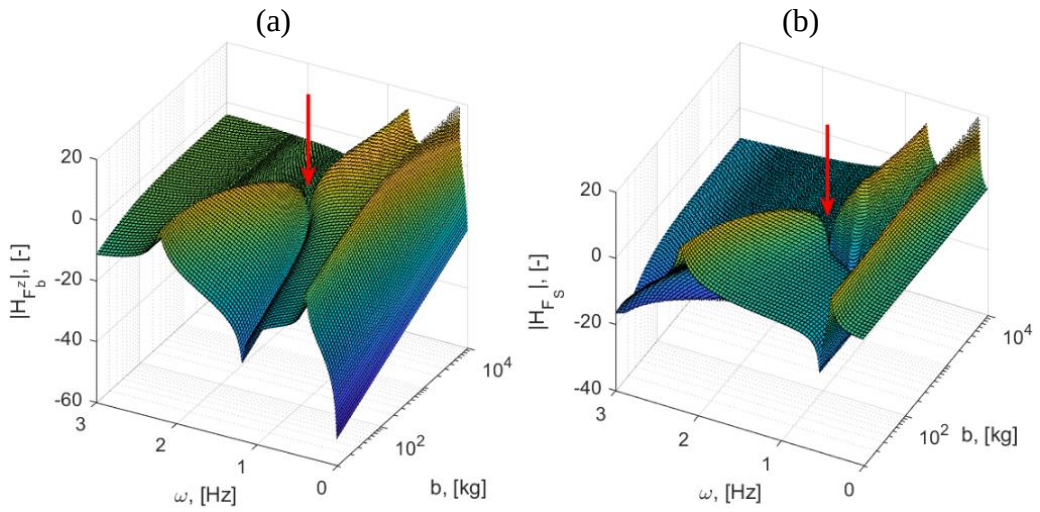

Figure 5 Transfer function showing the response of the contributing force components acting on the fuselage (orthographic projection). (a) Force through the inerter. (b) Shear force through the wing root.

As shown by the figure, a good match is obtained between the numerical and analytical anti-resonance frequencies, suggesting the validity of the approximations associated with Eq.(24). More importantly and coincidently, the antiresonance of the transmissibility functions H_{F_S} and $H_{F_b^{(z)}}$ (indicated by the dark blue regions in the figure) appear to intercept the resonant region at the same level of inertance as that of the antiresonance of the fuselage inertial force transmissibility, $H_{I_{fus}}$ (as seen in the encircled regions). This results in effectively suppressed resonant force transmission through the wing root and the inerter, at the same level of 'optimal' inertance at which the beneficial resonant and anti-resonant interactions were noted in $H_{I_{fus}}$. This is further illustrated in Figure *5*, for the resonant region arising from the second out of plane bending mode (B2), with the arrows indicating the annihilated resonance region at the inertance range at which the above behavior is noted.

To this end, it was shown that the studied inerter-based dynamic modification can be used to prompt resonant and anti-resonant interactions in the fuselage inertial force response, $H_{I_{fus}}$. This process is facilitated by the effects of modal flexibility (particularly that from higher frequency non resonant modes), which tend to place the nominal (inerter-free) anti-resonant frequency in the vicinity of the resonant frequency of the mode. In addition to this, the suppression of the resonant fuselage inertial force response ($H_{I_{fus}}$), through resonant and anti-resonant interactivity, was shown to be reflected by the individual force transmissibility functions H_{F_S} and $H_{F_b^{(z)}}$. The two-transmissibility function illustrated in Figure *4* entails individual force transmission paths whose aggregate results in the net fuselage inertial force investigated previously in Figure *3*. This suggests that the reduced $H_{I_{fus}}$ response is not achieved at the expense of an exacerbated force transmission through one of the possible transmission paths (inerter or wing root). The next section investigates this further, focusing on the relative phase and magnitude features of individual forcing components, to explore the redistribution of individual forcing components which yields this favorable behavior.

3.3 Inertance driven variation of internal shear force components

Obtaining simultaneous resonance and anti-resonance coalescence across multiple force transmissibility functions and at approximately the same inertance levels is particularly beneficial as this suggests the effective possibility of reducing the fuselage responses, hence improving ride comfort, without increased loads across the inerter and wing root. In order to visualize the varying composition of the involved forces, in both the magnitude and phase in the complex plane, Figure *6* shows the shear force equilibrium diagrams (polygons) of the participating force components at the B2 frequency and the selected values of the strut inertance.

The force diagrams essentially denote the individual force components defined in the complex plane under a unit harmonic input of F_{ext} as defined in Eq.(13). The closed nature of the polygonal loops is a result of the respective force balance conditions being satisfied – in this case approximately due to the small damping assumption. In this case, there are two diagrams considered, one related to the shear force balance on the wing itself (4-sided polygon suggesting $I_w = F_{ext} + F_S + F_b^{(z)} + I_w$), and the other obtained from the shear force balance of the fuselage (3-sided polygon suggesting $-I_{fus} = F_S + F_b^{(z)}$).

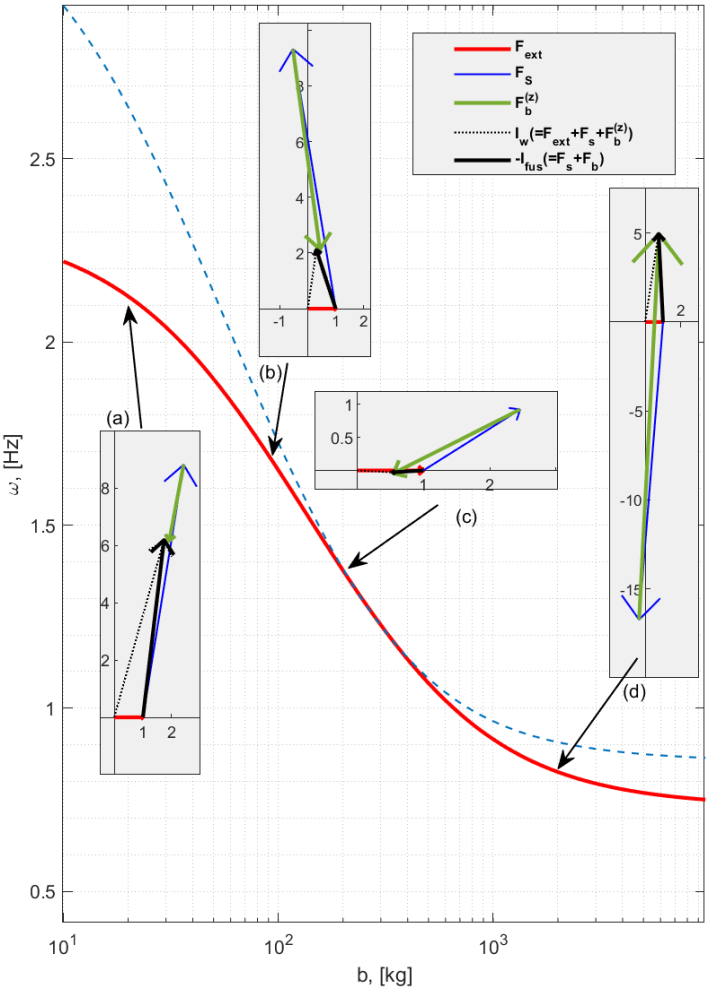

Figure 6 Complex force diagrams at the B2 frequency. The I_{fus} resonant and the anti-resonant frequencies in Figure 3 are indicated by the solid red and dashed blue lines, respectively.

A common feature seen across all the illustrated cases is the anti-phase placement of the wing root shear and the inerter forces, such that each of them essentially balance a component of the other. At low levels of inertance (case ‘a’), the wing root shear force component can be seen to be significantly amplified, in contrast to higher levels of inertance (case ‘d’) where the inerter force is larger in magnitude in comparison. As the fuselage-inertial force is a superposition of these two anti-phase components, the fuselage response is largely driven by the wing root shear force at low inertance levels. As the inertance is initially raised from lower levels (cases ‘a’ to ‘c’), the relative magnitude of the wing root shear components generally declines, resulting in a smaller net sum of the wing root shear and inerter forces in the region of resonance and anti-resonance interactivity (~case ‘c’). At the same time, the inertial response of the wing itself shows a similar qualitative characteristic, as this is essentially equal to the sum of the same wing root shear and the inerter force, with the constant unit excitation component. All in all, the observed reduction of the fuselage accelerance response at the ‘optimal’ inertance range does not appear to be one which arise at the expense of an amplified internal force transmission, or due to an amplified response of the wing acceleration itself.

4 CONCLUSIONS

This paper examined the fuselage accelerance response characteristics of a half-wing and fuselage configuration to identify useful inertia-driven features that enables certain resonant responses to be inhibited. It is shown that through strategic ‘inertial augmentation’, this can be realized by essentially enabling interactivity between an instance of anti-resonance and the targeted resonance region in frequency domain. Whilst the inertia-based augmentation in this case was realized through the inclusion of an inerter-based device, the analytical evaluation of the terms contributing to anti-resonance showed the possibility of encouraging this behavior by essentially tailoring the mass distribution (e.g., optimal fuel distribution) of the wing. In that case, the sensitivity exhibited by anti-resonance is predominantly a result of the flexibility effects of higher-frequency non-resonant modes. Additionally, in the context of the inerter-based realizations in the studied configuration, it was numerically shown that that this resonant response attenuation was achieved without the expense of amplified internal force components, but rather through an overall reduction of the structural load transmission.

Further development of this concept, which can be aimed at enhancing ride comfort and future considerations surrounding fuselage Hydrogen fuel storage, should address the combined influences from the aerodynamic sources (mass, damping and stiffness) and refined optimal criteria under complex interactions between elastic wing bending-torsion and fuselage pitching-plunging degrees of freedom.

ACKNOWLEDGEMENTS

The authors would like to kindly thank The UK Engineering and Physical Sciences Research Council (EPSRC) for funding this research project (Ref: 2625661), under grant number: EP/T517872/1.

REFERENCES

[1] Szczyglowski, C. P., Neild, S. A., Titurus, B., Jiang, J. Z., Coetzee, E. 'Passive Gust Loads Alleviation in a Truss-Braced Wing Using an Inerter-Based Device'. *Journal of Aircraft*, 2019, 56(6).

[2] Cheung, R. C. M., Rezgui, D., Cooper, J. E., Wilson, T. 'Testing of Folding Wingtip for Gust Load Alleviation of a Flexible High Aspect Ratio Wing'. *Journal of Aircraft*, 2020, 57(10).

[3] Li Y, Qin N. 'A Review of Flow Control for Gust Load Alleviation'. *Applied Sciences*. 2022, 12(20).

[4] Stevenson, J., Cheney, J. A., Usherwood, J. R., Bomphrey, R. J., Windsor, S. P. 'Dynamics of hinged wings in strong upward gusts'. *Royal Society Open Science*, 2023, 10(5).

[5] Mottershead, J.E., 'On the zeros of structural frequency response functions and their sensitivities', *Mechanical Systems and Signal Processing*, 1998, 12(5).

[6] Sanghi, D., Risi, C., Cesnik, C.E.S., *et al*., 'Analysis of ride qualities in transonic high-aspect-ratio-wing aircraft', *International Forum on Aeroelasticity and Structural Dynamics*, June 2022, Madrid, Spain.

[7] Richiedei, D., Tamellin, I., Trevisani, A. 'Beyond the Tuned Mass Damper: a Comparative Study of Passive Approaches to Vibration Absorption Through Antiresonance Assignment'. *Arch Computational Methods Eng*, 29.

[8] Frahm H (1911) Device for damping vibrations of bodies. US Patent 989,958.

[9] I. Bucher, S. Braun, 'The structural modification inverse problem: an exact solution'. *Mechanical Systems and Signal Processing*, 1993, 7(3).

[10] Ma, R., Bi, K., Hao, H., 'Inerter-based structural vibration control: A state-of-the-art review', *Engineering Structures*, 2021, 243.

[11] Patil, M. J., Hodges, D. H., 'Flight Dynamics of Highly Flexible Flying Wings', *Journal of Aircraft*, 2006. 43(6).

COPYRIGHT STATEMENT